Research papers

Temporal and spatial variation in shallow groundwater gradients in a boreal headwater catchment

Jana Erdbrügger [a,*], Ilja van Meerveld [a], Jan Seibert [a,b], Kevin Bishop [b]

[a] *Department of Geography, University of Zurich, Zurich, Switzerland*
[b] *Department of Aquatic Sciences and Assessment, Swedish University of Agricultural Sciences, Uppsala, Sweden*

ARTICLE INFO

ABSTRACT

In humid climates, shallow groundwater is often assumed to be a subdued replica of the surface topography. Nevertheless, the relation between the surface topography and groundwater table can change over time, especially when catchment wetness changes. To investigate the correlation between the surface topography and the groundwater table, we analyzed groundwater levels and gradients in a boreal headwater catchment using 1.5 years of continuous groundwater level data for 75 wells. As expected, groundwater gradients changed with catchment wetness. Gradient directions calculated over short distances (5 m) changed by up to 360°; gradients calculated over larger distances (20 m) varied by up to 270°. The groundwater gradient directions were generally most variable for flatter locations and locations where the local surface slope differed from the surrounding topography. Smoothed digital elevation models (DEMs) represented the groundwater surface better than high-resolution DEMs. The optimal degree of smoothing varied over the year and was lowest for very wet periods, such as the snowmelt period, when groundwater tables were high.

1. Introduction

In humid climates, the groundwater table is often assumed to be a subdued replica of the topographic surface. Thus, when no or only limited groundwater level data are available, and there are no known geological constraints on water movement, a smoothed version of the surface topography is often used to approximate the shape of the groundwater table and to infer groundwater flow directions (Condon and Maxwell, 2015; Haitjema and Mitchell-Bruker, 2005; Tóth, 1962; Winter, 1999). However, shallow groundwater gradients vary over time, and the groundwater table is a more subdued version of the surface topography when groundwater levels are low (Winter, 1999). Thus, in an area with undulating topography, the flow directions can be towards local depressions during wet conditions and towards the main valley during dry conditions (e.g., Winter, 1999). This implies that differently smoothed topographic models of the catchment are needed to approximate groundwater flow directions at different times. Hitherto, there is no clear advice on which digital elevation model (DEM), i.e., what degree of smoothing or resolution, best describes the shape of the groundwater table or how this changes with wetness conditions (Erdbrügger et al., 2021), even though this will affect the simulated

groundwater flow pathways, and thus the simulated contribution of groundwater to streamflow, pollutant transport, and even the size of the groundwater catchment.

This lack of guidance on what degree of DEM smoothing to use to represent the groundwater table is partly caused by the lack of high-spatial-resolution groundwater measurements. Spatially distributed groundwater level data have only been collected in a few research catchments. Despite the large number of wells involved in these studies, the resolution was usually still not sufficient to allow interpolation of the measurements to determine the direction of the groundwater table. For example, Rinderer et al. (2014) measured the water level in 51 wells in the 20-ha Studibach catchment in Switzerland. The average density of 2.6 wells/ha results in an average distance of 62 m between each well if they were placed at equal distances. A similar calculation would result in an average distance of 26 m between the 59 wells used in the study by Moore and Thompson (1996), 877 m for the > 100 wells in the study of Myrabø (1997), and 7 m for the 22 wells in the study of Bonanno et al. (2021). Several studies have collected high-spatial-resolution groundwater data for individual hillslopes. The average distance between piezometers was 2 m for a hillslope at the Panola Mountain Research Watershed (Tromp-van Meerveld and McDonnell, 2006), 3 m for wells

---

* Corresponding author.
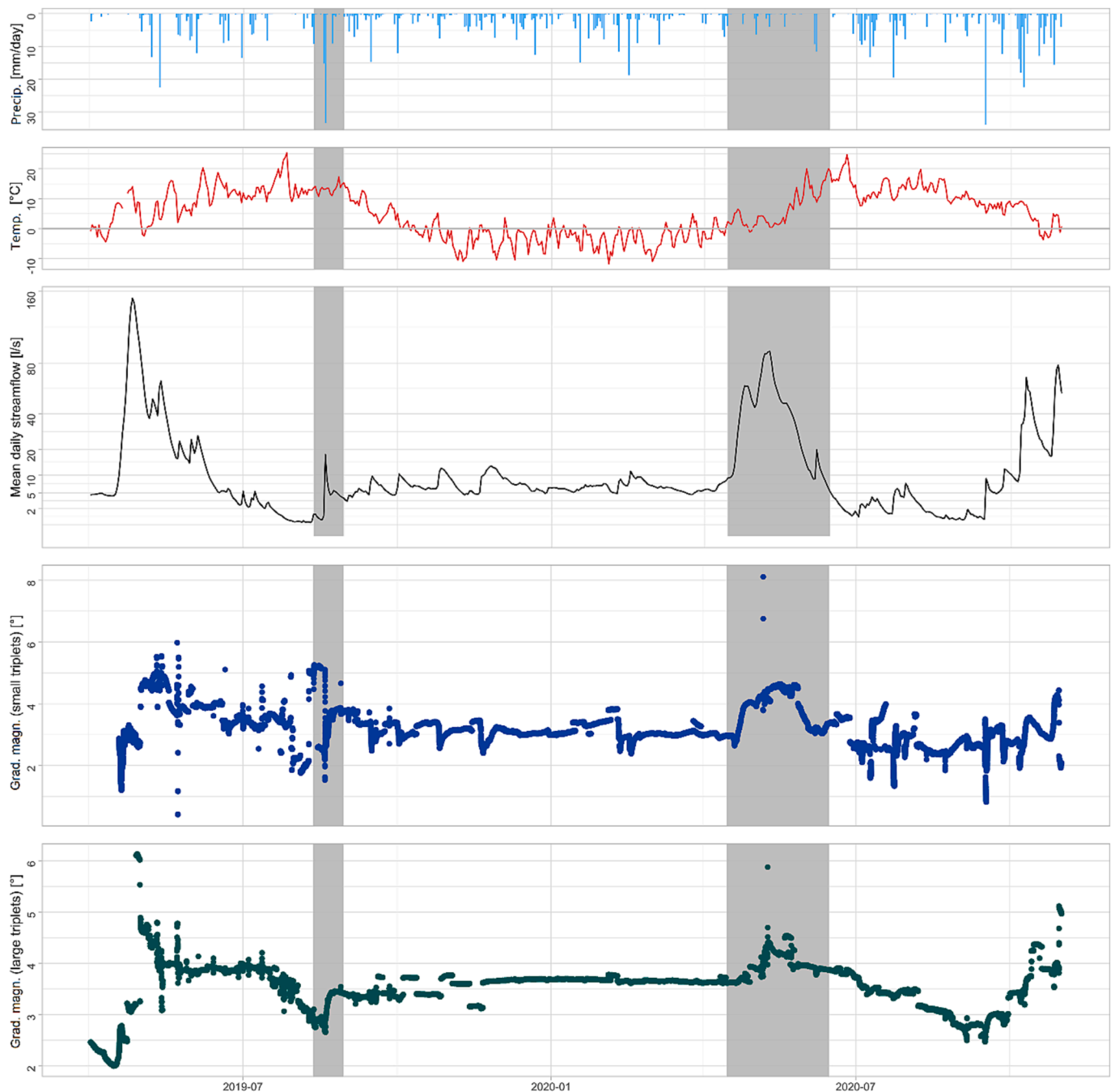*E-mail address:* jana.erdbruegger@geo.uzh.ch (J. Erdbrügger).

Fig. 1. Time series of daily precipitation (rainfall and snowfall), daily average air temperature, and mean daily streamflow from the C6 gauging station (i.e., the stream draining area A) and the average gradient magnitude of the groundwater table (θ) calculated for all small and large triplets between April 2019 and October 2020. The time series clearly show the snowmelt peaks in May 2019 and 2020, and the streamflow in response to large precipitation events in September and October 2020. The gray shaded areas represent the periods shown in Figs. 2 and 3. Note that the streamflow is plotted on a square root scale to better visualize the high and low flows.

on multiple transects for hillslopes in Southern Germany (Bachmair et al., 2012), and 3.5 m for wells on a hillslope in the Malcolm Knapp Research Forest (Haught and van Meerveld, 2011). Although these studies collected high-resolution groundwater level data, the measurement networks were not designed to answer questions related to the direction of the groundwater table or what degree of DEM smoothing best approximates the groundwater table at different times. The effect of the choice of the DEM or the resolution of the DEM for hydrological modeling has been tested in other studies (e.g., Lagacherie et al., 1996; Moges et al., 2023; Wise, 2007) but these results were not interpreted with respect to the groundwater flow patterns.

The few field studies where groundwater flow directions have been calculated show that the surface topography does not always represent the groundwater flow directions and that the flow directions can change considerably over time. For example, Hinton et al. (1993) found for a glacial till catchment in Canada that the shallow groundwater levels were not always perpendicular to the surface contours and highlighted that this caused the boundary of the groundwater watershed to be different from the surface topography based catchment boundaries. Similarly, Molénat et al. (2005)showed that for the midslope and up-slope location in their catchment in Brittany, France, with silty loam soils, the groundwater flow directions were never aligned with those of
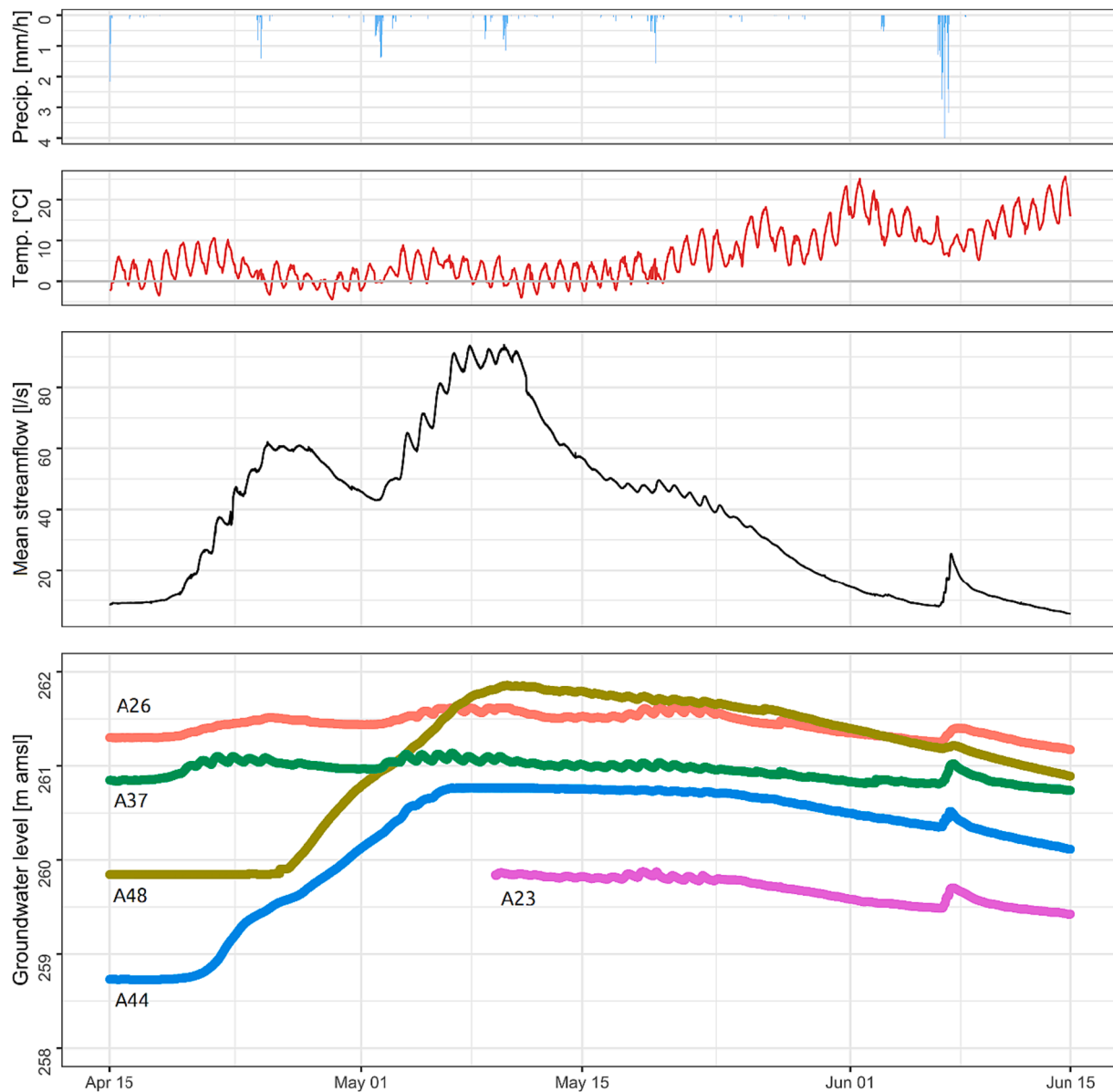
Fig. 2. Time series of precipitation, air temperature (30 min data), and streamflow and groundwater levels for selected wells (labels indicate the well number) (10 min data) during the 2020 snowmelt period (mid-April –June 2020).

the surface topography derived from a 2 m DEM. They highlight that this has important implications for the representation of the groundwater in catchment scale hydrological models (Molénat et al., 2005).

Other studies highlighted the variability in flow directions. Rodhe and Seibert (2011) and von Freyberg et al. (2014), for example, found that flow directions at foot slopes and riparian sites were towards the stream when water levels were high but parallel to the stream during drier periods. In near stream areas, groundwater flow directions can even switch from the hillslope towards the stream to the opposite direction (i.e., from the stream into the riparian zone; Vidon, 2012; Vidon and Smith, 2007; Wroblicky et al., 1998). Other studies concluded that the groundwater flow directions were similar to those of the surface topography when groundwater levels were high but that they were better aligned with the topography of the soil–bedrock interface (van Meerveld et al., 2015) or the top of the C horizon (Benton et al., 2022) during drier conditions. In the study by Rodhe and Seibert (2011) flow directions varied by up to 56°, in the study by Benton et al. (2022) by up to 75°, and in the study by van Meerveld et al. (2015) by up to 90°.

Recently, high-resolution shallow groundwater level data and

topographic data have been collected in the Krycklan catchment in northern Sweden (Erdbrügger et al., 2023). These data provide an opportunity to study the variability in groundwater gradients and to test which resolution DEM best represents the observed gradients (in terms of direction and magnitude). Erdbrügger et al. (2021) found that for a considerable part of this catchment, the direction of the surface topography depends on the degree of smoothing of the DEM. The circular variance (C_v) was high ($C_v > 0.104$) for 24 % of the catchment and very high ($C_v > 0.378$) for 6 % of the catchment. Especially for areas near the stream channel, on the ridges, and in flat areas, the derived flow directions were highly sensitive to the degree of DEM smoothing or aggregation. Therefore, in this study, we used real groundwater level data from the dense monitoring network to address the following research questions:

1. How variable are groundwater gradients throughout the year, and does this variability depend on the spatial resolution over which it is assessed?
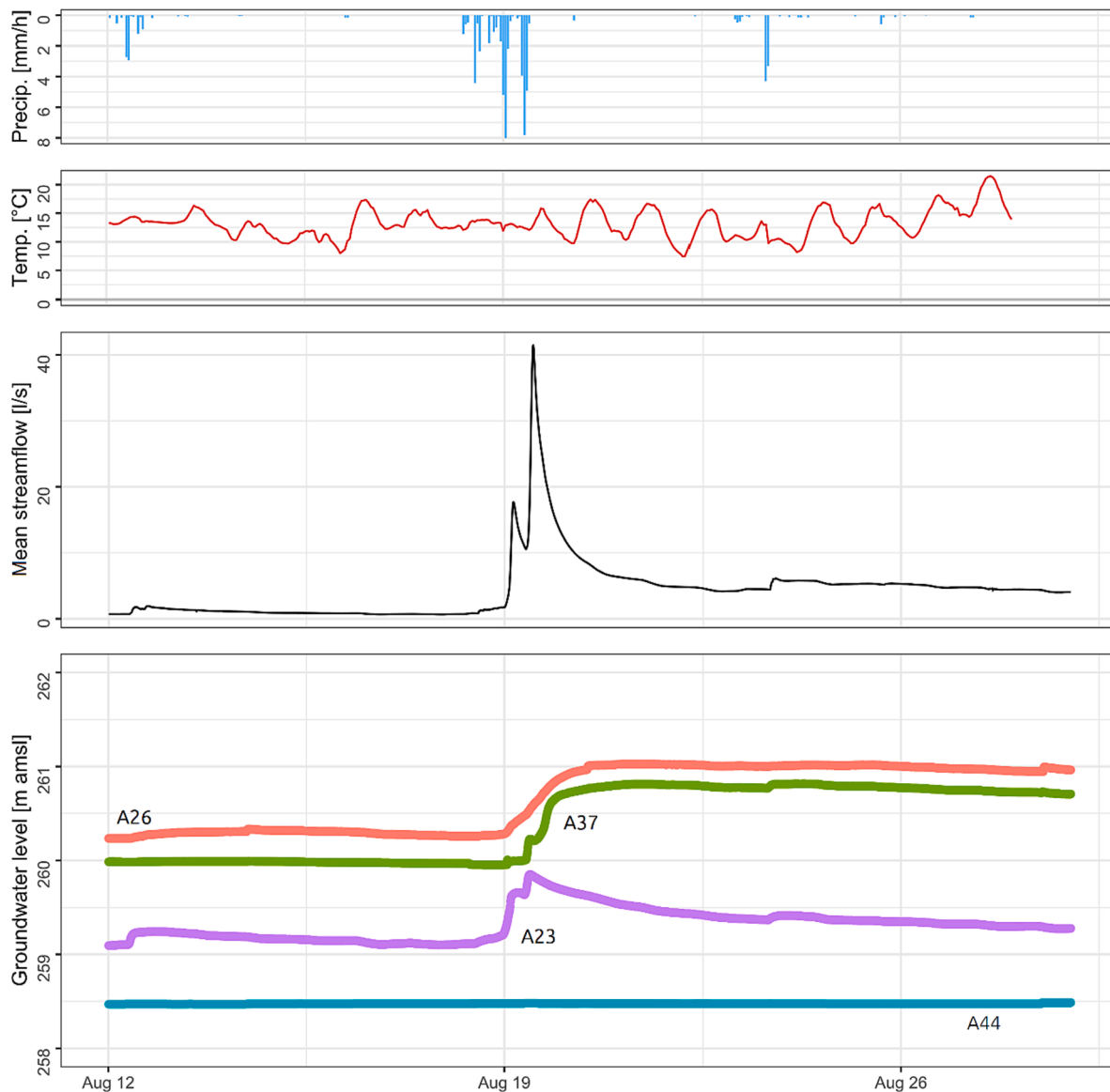
Fig. 3. Time series of precipitation and temperature (30 min data), and streamflow and groundwater levels for selected wells (labels indicate well number) (10 min data) during precipitation events after an extended dry period in August 2019,

2. Are flow directions most variable for near-stream areas, flat areas, and ridges (i.e., for the sites for which the calculated flow directions based on differently smoothed DEMs differed the most)?

3. What degree of DEM smoothing best describes the observed flow directions, and does this depend on wetness conditions?

2. Study area

The high spatial and temporal resolution groundwater data used in this study were collected in wells installed in two sub-catchments of the Krycklan research catchment, located in northern Sweden, approximately 50 km west of Umeå (Laudon et al., 2021, 2013). Area A is located in what is referred to in other studies as catchment C6 (0.44 km^2), while area B is a hillslope in a catchment that is known as C2 (catchment: 0.12 km^2; hillslope: 0.01 km^2) and includes an area called the S-transect. The elevation of the study areas varies between 250–270 m a.m.s.l.. Groundwater flow at Krycklan is a nested system with shallow and deeper groundwater flow pathways (Kolbe et al., 2020). Groundwater tables in the Krycklan catchment are generally shallow (<6 m from the surface, and in most locations < 2 m), and groundwater

level fluctuations in the riparian zone are well correlated with the stream level (Seibert et al., 2003).

The majority of the study area is covered by Scots pine (Pinus sylvestris) or Norway spruce (Picea abies) forest (Laudon et al., 2021, 2013). The study area is characterized by till soils, but some bedrock outcrops also exist. Peat has formed in the wetter lower ends of the slopes. Area A contains several peatland patches and streams, as well as some small ridges and several hillslopes with a differing inclination. Area B is a hillslope with some peaty patches and has slopes that are less variable than in area A. The average gradient is 6.5° (range: 0.1–26.7°) for area A and 5.0° (range: 0.1–15.3°) for area B.

The region has a cold temperate humid climate and is covered with snow during winter. The 30-year mean annual temperature (1981–2010) is 1.8 °C and varies between −9.5 °C in January and 14.7 °C in July. Mean annual precipitation is 614 mm/y, of which on average 30 % falls as snow. Mean annual streamflow is 311 mm/y, resulting in a derived mean annual evapotranspiration of about 300 mm/y (Laudon et al., 2021, 2013). The groundwater measurements were taken between April 2019 and October 2020, and thus, included two snowmelt seasons. The summer of 2019 was particularly dry (total
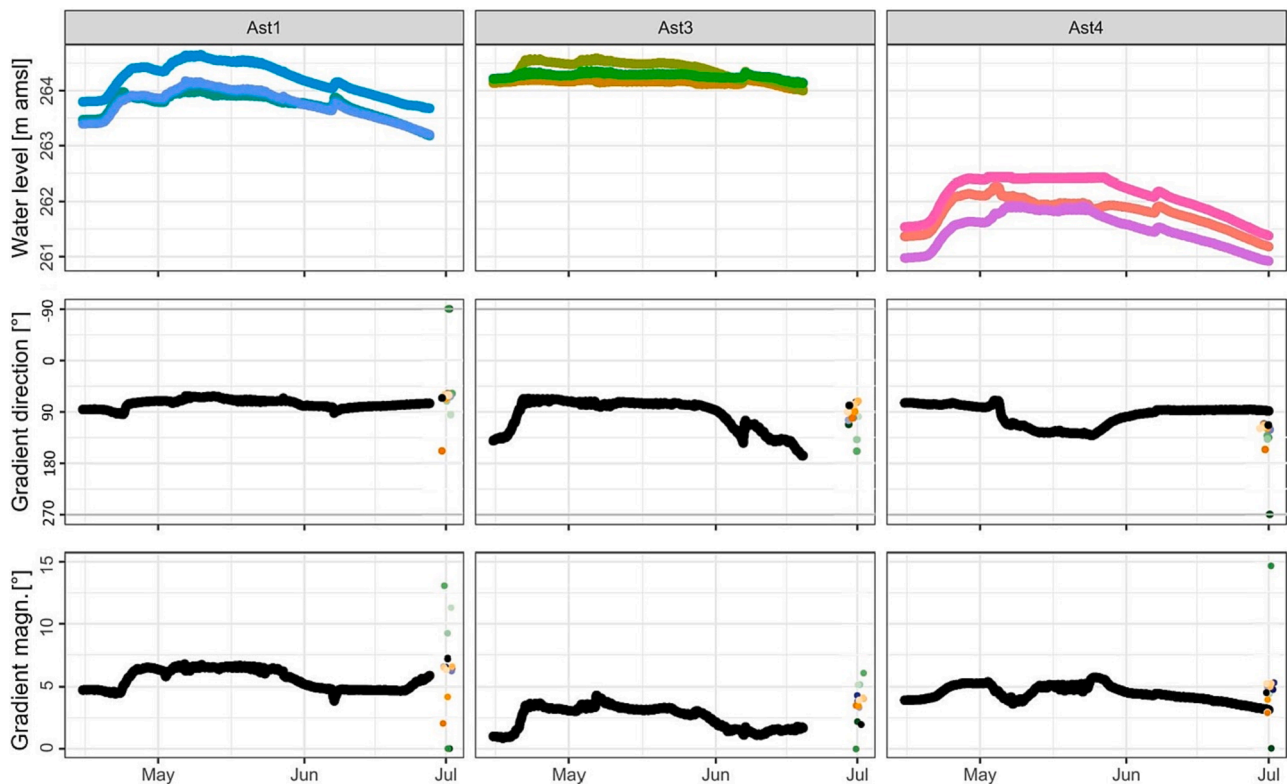
Fig. 4. Time series of groundwater levels (top row), gradient directions (middle row), and gradient magnitude (lower row) for three selected small triplets during the snowmelt period between mid-April - June 2020. The gradient direction and magnitude of the surface topography derived from the smoothed DEMs are indicated on the right side of the graphs (black for the original DEM, orange for Gaussian filter, blue for Mean filter, green for aggregated DEMs, lighter colors indicate stronger smoothing, see Table C1). For the location of the selected triplets, see Fig. 6. (For interpretation of the references to colour in this figure legend, the reader is referred to the web version of this article.)

precipitation of 29 mm in July (long-term average 68 mm).

3. Methods

3.1. Field measurements

The 75 wells were installed during summer (May – July) 2018 and winter (February-March) 2019: 54 wells in study area A and 21 in study area B, leading to a density of 15 wells per ha for area A and 20 wells per ha for area B. All the 3.7 cm diameter wells were installed in the till. The average depth of the wells was 274 cm (range: 57–578 cm). The wells were placed in such a way that they formed either small (5 m) or large (20 m) triangles to allow for the calculation of the groundwater table gradient (see section 3.2.1. Field data analysis). We call the three wells that form a triangle a *triplet* (see Table S1 for a complete list of all triplets). We used small and large triangles because we expected the calculated gradients and their variability to depend on the scale over which the gradients are calculated and the related degree of smoothing. More specifically, we expected micro-topography to have a larger effect on the shape of the groundwater table at the small scale and that these differences are smoothed out more at the 20 m scale of the larger triangles.

In each well, a capacitance water level sensor (Dataflow Systems Ltd, 2021) was installed to record the groundwater level at 10 min intervals. Water levels were also measured manually weekly to biweekly from May to September 2019 and 2020. Water levels were measured up to 26 times for each well, but for almost half of the measurements, the wells were dry (i.e., the groundwater level was below the bottom of the well), so the average number of manual groundwater level measurements per well was 14. These manual water level measurements were used to correct the offset between the logger data and the measured water levels.

The elevation of the well tops was determined by geo-referencing a terrestrial laser scan (TLS Trimble TX8, Sunnyvale, USA). This allowed us to determine the absolute water levels (in m above mean sea level (m a.m.s.l.)) for each well and time step. A more detailed description of the study area, the installation and maintenance of wells and sensors, and the groundwater level data can be found in Erdbrügger et al. (2023).

Climate data for the study period were obtained from the ICOS (Integrated Carbon Observation System, ICOS, 2021) station, located < 500 m from the study sites. Streamflow data were obtained from Laudon et al. (2021, 2013).

3.2. Field data analysis

We used the absolute groundwater level for each well to calculate the gradient (both the magnitude (θ) and the direction (α)) between the three wells of each triplet. This calculation assumes that the local groundwater surface can be described by a triangle defined by three groundwater levels (cf. Rodhe and Seibert (2011) and van Meerveld et al. (2015)) (see Appendix A: Gradient calculations, Equations A1–A4). We assume that the calculated gradients mainly represent the local groundwater system because of the very shallow groundwater levels and the small scale of the triangles and watershed. For the display of the results, we determined the centroid of each triplet (see Equation A(5). Directions in the text are given in degrees clockwise from 0° - North (90° = East, 180° = South, 270°/-90° = West).

We calculated the gradients (direction and magnitude) for all time steps for which data were available for all three wells. Because there were gaps in the water level measurements for some triplets, either due to logger malfunctioning or because the water level dropped below the bottom of one (or more) of the well(s), we excluded triplets for which we had less than two weeks of complete data. At a 10 min interval, this
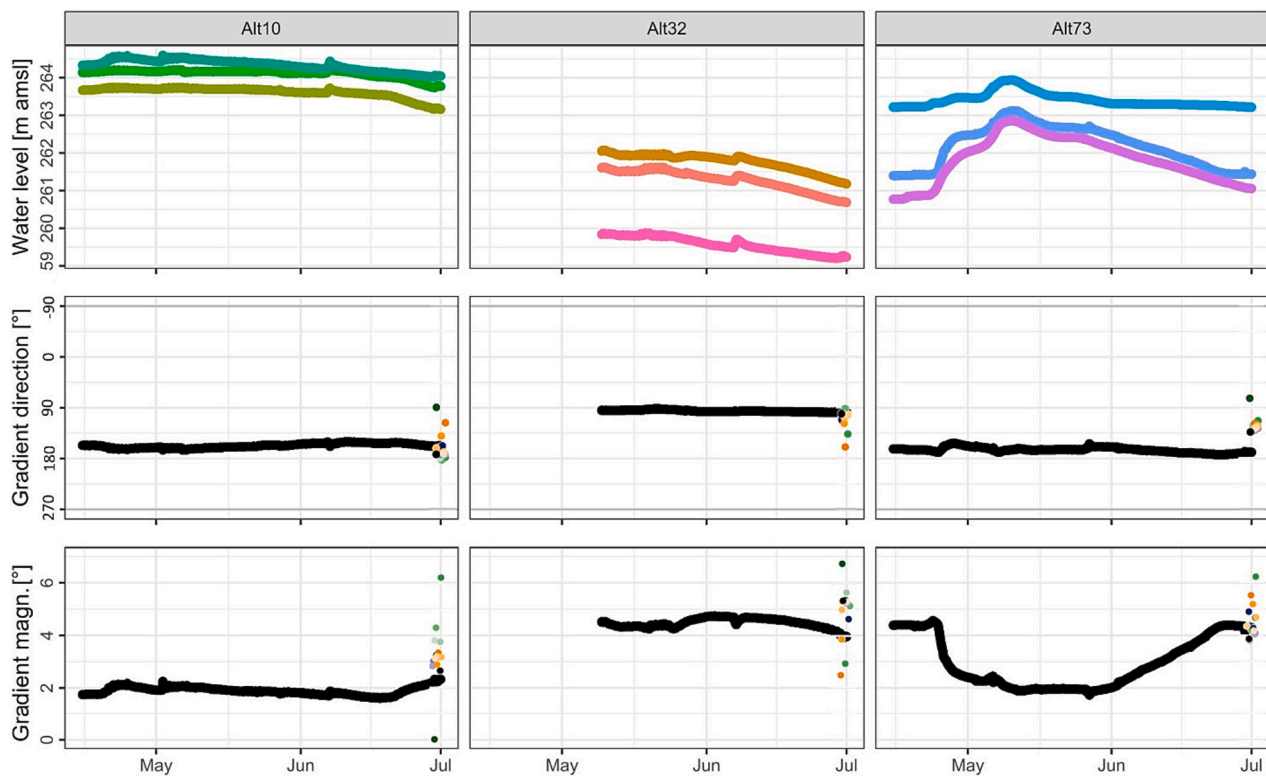
Fig. 5. Time series of groundwater levels (top row), gradient direction (middle row), and gradient magnitude (lower row) for three selected large triplets during the snowmelt period between mid-April - June 2020. The gradient direction and magnitude of the surface topography derived from the smoothed DEMs are indicated on the right side of the graphs (black for the original DEM, orange for Gaussian filter, blue for Mean filter, green for aggregated DEMs, lighter colors indicate stronger smoothing, see Table C1). For the location of the selected triplets, see Fig. 6. (For interpretation of the references to colour in this figure legend, the reader is referred to the web version of this article.)

results in at least 2016 coinciding measurements per triplet (see Appendix B, Table B1 for the actual number of measurements for each triplet). In total, we included data for nine small triplets (7 in area A and 2 in area B) and 94 larger triplets (53 in area A and 41 in area B).

For each triplet, we calculated the circular variance C_v as a measure of the variability in the gradient directions. The circular variance is the inverse of the length of the mean resultant vector (Erdbrügger et al., 2021; Pewsey et al., 2013) and is similar to the linear variance. We hypothesized that the gradient directions would be more variable for the smaller triplets because of the larger effect of microtopography and reduced smoothing. We used the same threshold to define a high variability ($C_v = 0.104$) as Erdbrügger et al. (2021). This circular variance represents evenly spaced vectors within a 45° range. We calculated the circular variance for each month and a one-year study period (July 2019-June 2020). As the snow melt period is usually the time of highest streamflow in the study area (e.g., Laudon et al., 2021, 2013), we looked more closely at the groundwater levels and gradients during the snow-melt periods (mid-April to June).

We calculated the arithmetic average of the gradient magnitude for the small and the large triplets and related this average magnitude to the streamflow as a measure of catchment wetness. We expected the slope of the groundwater table to be steeper during wet periods, when ground-water levels and streamflow are high, and less steep in drier periods. We, furthermore, determined for each triplet the relation between the average water level (for the three wells), the gradient magnitude, and the gradient direction because previous studies showed that ground-water gradients depend on the groundwater level (e.g., Rodhe and Seibert, 2011; van Meerveld et al., 2015; von Freyberg et al., 2014).

We also expected to see more pronounced changes in the direction of groundwater flow when the gradient magnitude is smaller (because small changes in the water level for one well then cause a more pronounced change in the gradient direction). We, therefore, compared the variation in the gradient direction (i.e., the circular variation) over the one-year period with both the mean gradient magnitude of the groundwater table and the surface slope.

3.3. Comparison to DEM-based gradients

We compared the observed gradients for each triplet to those of the surface topography to determine how well the surface topography reflects the shape of the groundwater table and, thus, to test the assumption that the groundwater table is a subdued copy of the surface topography. For this, we used the LiDAR-derived DEM of the Krycklan catchment (Laudon et al., 2021, 2013) with a 2 m by 2 m resolution processed for hydrological modelling (removal of sinks; named *original* in the remainder of the text). We also used all 15 DEMs that were smoothed or resampled to a lower resolution of Erdbrügger et al. (2021). The smoothed DEMs are created by filtering the original DEM with a Gaussian filter with differing weighted means of the surrounding pixels (DEMs referred to by *gauss$_n$*, where *n* refers to the number of pixels used for the calculation of the standard deviation, varying between 2 and 20), a mean filter with differing window size (DEMs refered to by *mean$_n$*, where, *n* refers to the number of pixels used for calculating the mean, varying between 3 and 21), and by aggregating pixels (DEMs refered to as *agg$_n$*, where *n* refers to the number of aggregated pixels, varying between 2 and 20) (for details see Erdbrügger et al. (2021) and Appendix C).

We hypothesized that the groundwater is a smoother version of the surface topography during drier times than during wet times and that the more smoothed DEMs would thus represent the actual groundwater gradients better during the drier periods. Therefore, we extracted the gradient (magnitude and direction) for the pixel in the centroid of the
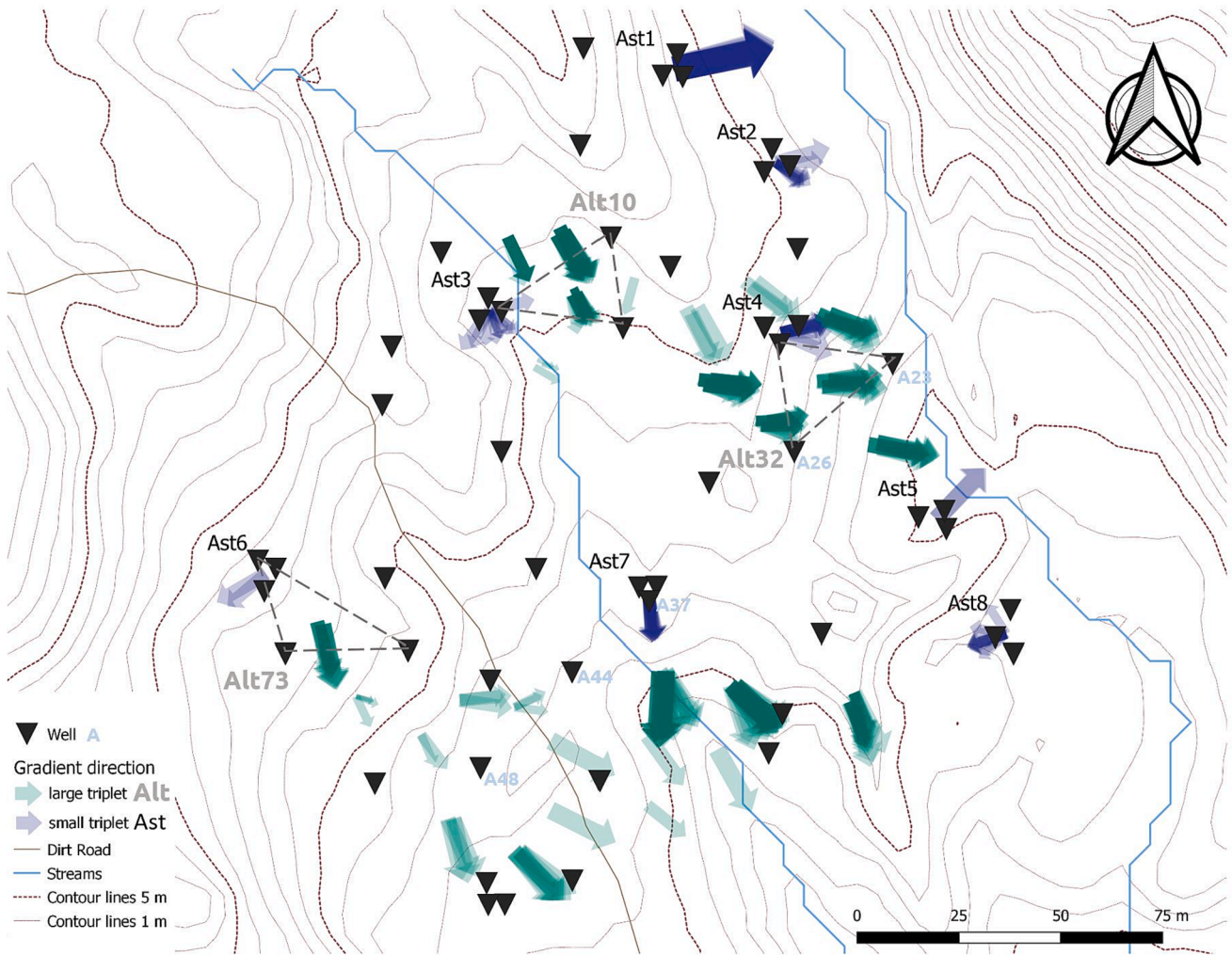
Fig. 6. Map showing the monthly mean gradient directions for the large (green) and small (blue) triplets. Each arrow represents one month between July 2019 and June 2020. The size of the arrow represents the average gradient magnitude for that month (smaller means less steep). More intense colors mean more overlapping arrows. Labels next to the arrows, indicate the name of the triplet for which the groundwater level data and gradients are shown in Fig. 4 and Fig. 5. (For interpretation of the references to colour in this figure legend, the reader is referred to the web version of this article.)
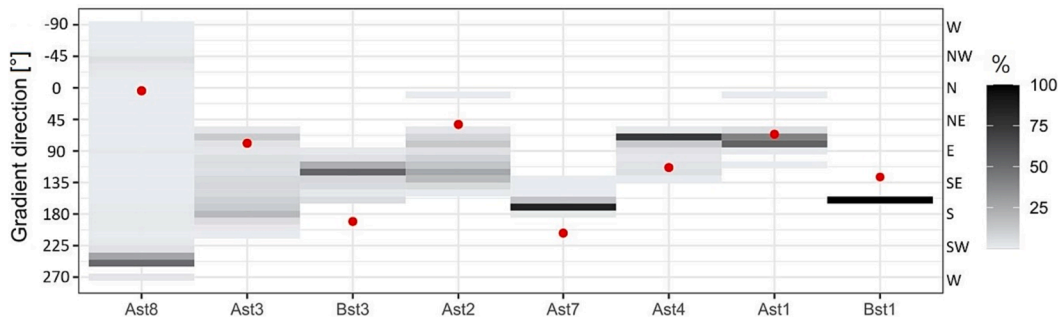

Fig. 7. Distribution of the gradient directions between July 2019 and June 2020 for all small triplets. The gray shading indicates the percentage of all measurements for which the gradient direction was within a specific 10° class (see Table S1 for the total number of measurements for each triplet). The triplets are ordered by the mean gradient magnitude (Ast8 lowest to Bst1 highest). The red dots indicate the gradient directions of the surface topography for each triplet based on the original DEM. (For interpretation of the references to colour in this figure legend, the reader is referred to the web version of this article.)

triplet for each DEM and compared this gradient to the calculated mean groundwater gradient. Again this was done for each month, the snowmelt period, and the one-year study period. More specifically, we determined for each period and triplet which DEM best represented the gradient direction (i.e., for which DEM the difference between the gradient direction of the DEM and the mean gradient direction derived

from the groundwater levels was smallest). The DEM that represented the gradient direction best for most triplets was considered the best DEM to represent the groundwater table direction for that period. We did this separately for the small and large triplets because we assumed that microtopography would have a larger influence on the groundwater table at the small scale, and that a less smoothed DEM would therefore
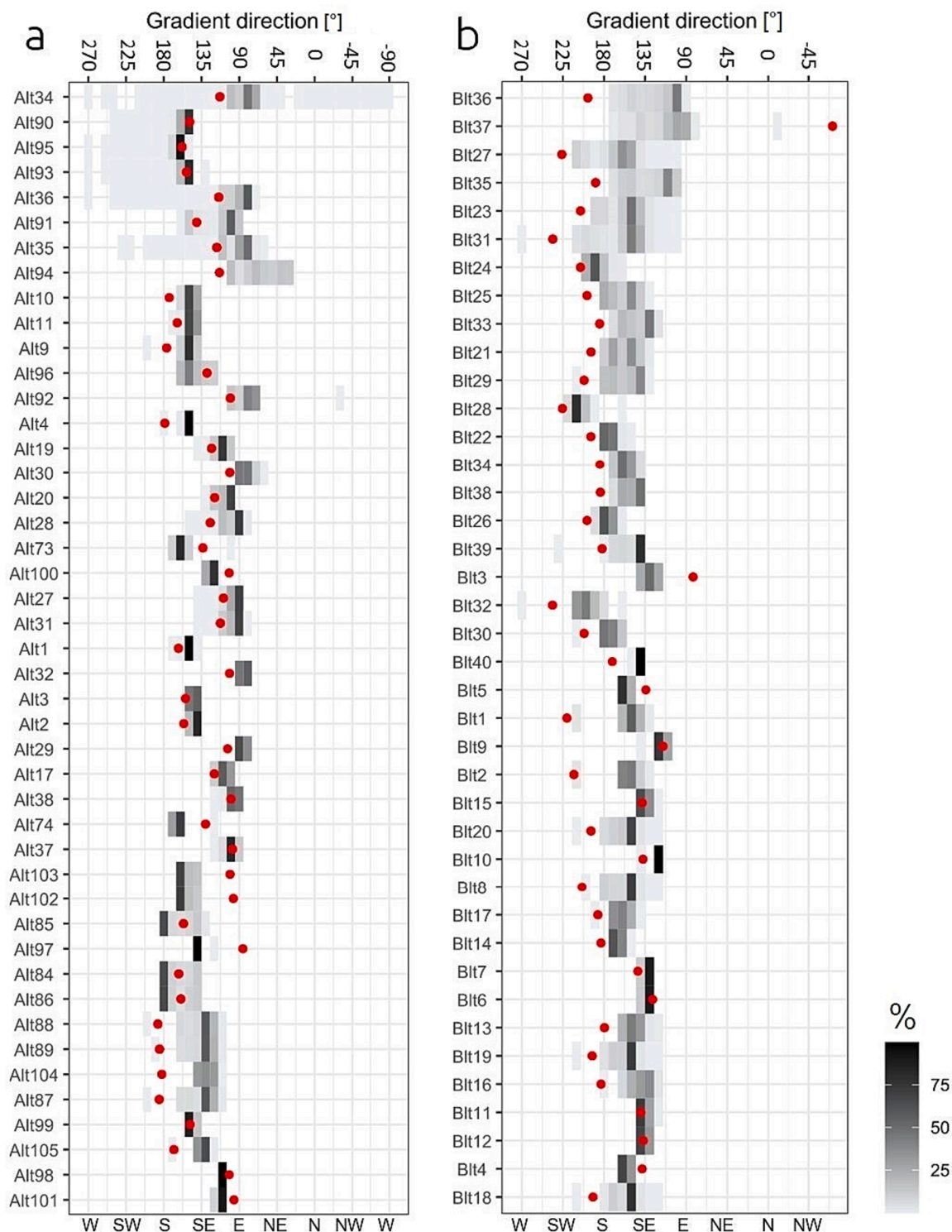
Fig. 8. Distribution of the gradient directions between July 2019 and June 2020 for all large triplets in area A (a) and area B (b). The gray shading indicates the percentage of all measurements within a 10° direction class (see Table S1 for the total number of measurements for each triplet). The triplets are ordered by the mean gradient magnitude (lowest (top) to highest (bottom)). The red dots indicate the gradient direction of the surface topography for each triplet based on the original DEM. (For interpretation of the references to colour in this figure legend, the reader is referred to the web version of this article.)

represent the small scale groundwater variations better. We expected these variations to level out over larger scales, and that the groundwater gradients for the larger scale would therefore be better represented by the more smoothed DEMs.

To determine whether the locations for which the groundwater gradient directions are most variable can be predicted based on the variation of the gradients calculated for the different DEMs (i.e., DEMs with different levels of smoothing), we compared the monthly circular variance (C_V) with to those obtained for the 15 different DEMs (i.e., those calculated by Erdbrügger et al. (2021)).
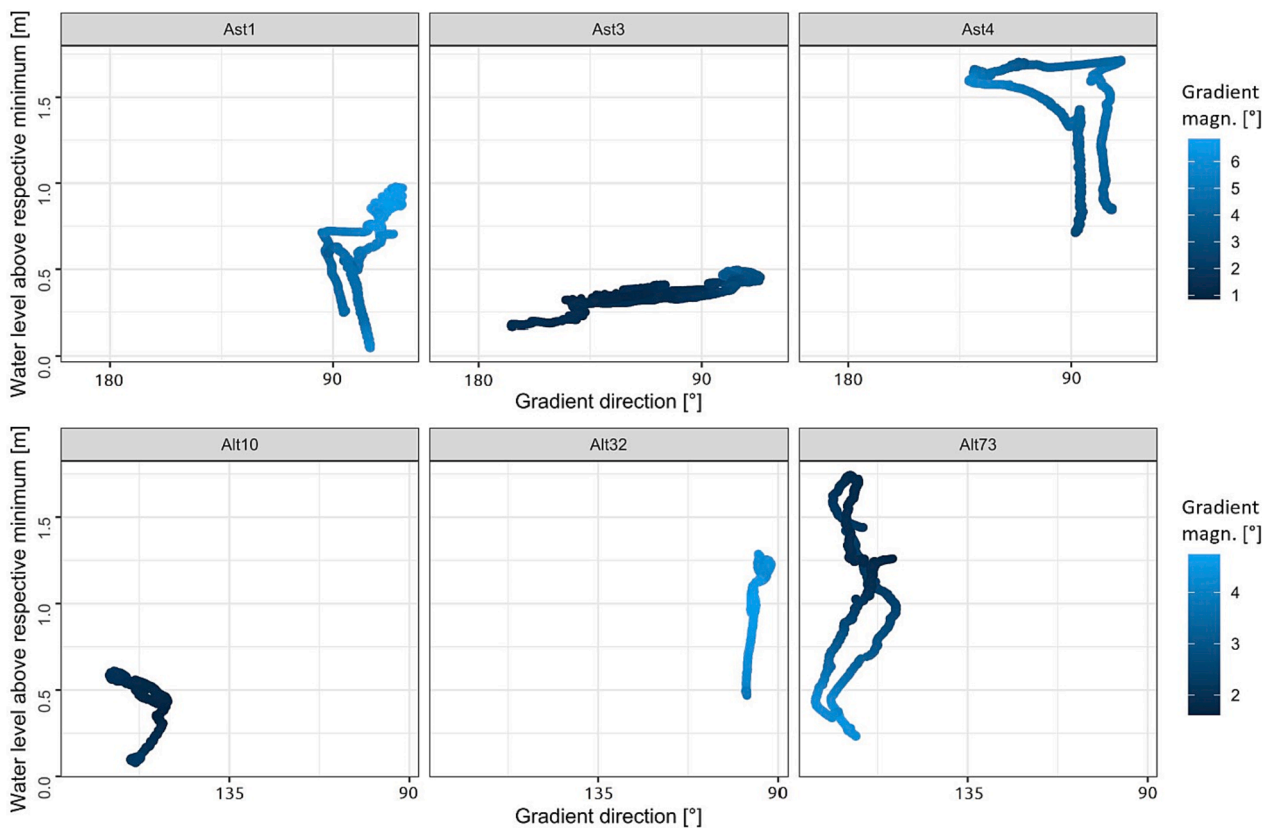
Fig. 9. Relation between the mean water level of a triplet above the minimum measured level (in m), gradient direction, and gradient magnitude (in degrees) during the 2020 snowmelt period (mid-April -June 2020) for three small (top) and three large (bottom) triplets.

4. Results

4.1. Groundwater level dynamics

Streamflow and groundwater levels increased during the snowmelt periods of April to June 2019 and 2020 (Figs. 1 and 2). Peak groundwater and streamflow occurred in both years in mid-May. The amplitude of the groundwater level rise mainly depended on how close the groundwater level was to the surface at the start of the snowmelt. For most wells there were diurnal variations in the groundwater level during the snowmelt period (Fig. 2). Precipitation events during the summer and fall also led to a groundwater level response but the increases were less pronounced than during the snowmelt period. The timing of the peak water level and the change in water level varied between wells (Fig. 2-Fig. 3), with the deeper wells located further from the streams generally reacting slower than the other wells.

4.2. Groundwater gradients

4.2.1. Gradient magnitude

The average magnitude of the gradient of the groundwater table (average for all triplets) was larger during periods with high streamflow than during other periods (Fig. 1). The Spearman rank correlation between streamflow and the average gradient magnitude was 0.26 for the small triplets and 0.46 for the large triplets (p-value very small due to the large number of data points (i.e., all measurement times)). However, the changes in the gradient magnitude differed for the different triplets (Figs. 4–6). The gradient magnitude of the groundwater table changed more during rainfall events for the small triplets than for the large triplets (Fig. 1). Still, the overall range (0.2–8.1° for the small triplets and 2.0°-6.1° for the larger triplets) and average gradient magnitude (3.2° for the small triplets and 3.5° for the larger triplets) were similar.

4.2.2. Gradient direction

The groundwater gradient directions varied strongly for some triplets but were more stable for others (Fig. 6). For only one of the nine small triplets and none of the 94 large triplets was the circular variance of the groundwater gradient direction (C_v) larger than 0.104 (our threshold for a high C_v, and thus large variation in gradient direction) when C_v was calculated over the entire year. The Spearman's rank correlation between the annual C_v and mean groundwater gradient magnitude was −0.78 (p < 0.001; see Figs. 6–8). The average Spearman rank correlation between the monthly C_v and the gradient magnitude of the surface topography was −0.58 (p < 0.001) for the small triplets and −0.11 (p < 0.001) for the large triplets. These results indicate more stable groundwater flow directions for steeper sites, where the groundwater table was steeper. However, there was no correlation between monthly C_v and the average Topographic Wetness Index (TWI) for a triplet (Spearman rank correlation of 0.02 (p = 0.75) for the small triplets and −0.06 (p = 0.05) for the large triplets).

The variability in the gradient direction (as represented by the average C_v) was highest in April 2020. The monthly circular variance was considered high ($C_v > 0.104$) for two small triplets but none of the large triplets in June 2019 and February, April, September and October 2020. For none of the triplets was the C_v high in July, September and October 2019 and January, May, July and August 2020.

The gradient direction did not change in a monotonic way with the average groundwater level for most triplets. Instead, for most triplets the relation was hysteretic during the snowmelt period (see examples in Fig. 9). There was also no clear relation between the average C_v and the monthly average discharge, nor the variation in discharge (Fig. 10).

4.3. Comparison of flow gradients with those derived from the DEMs

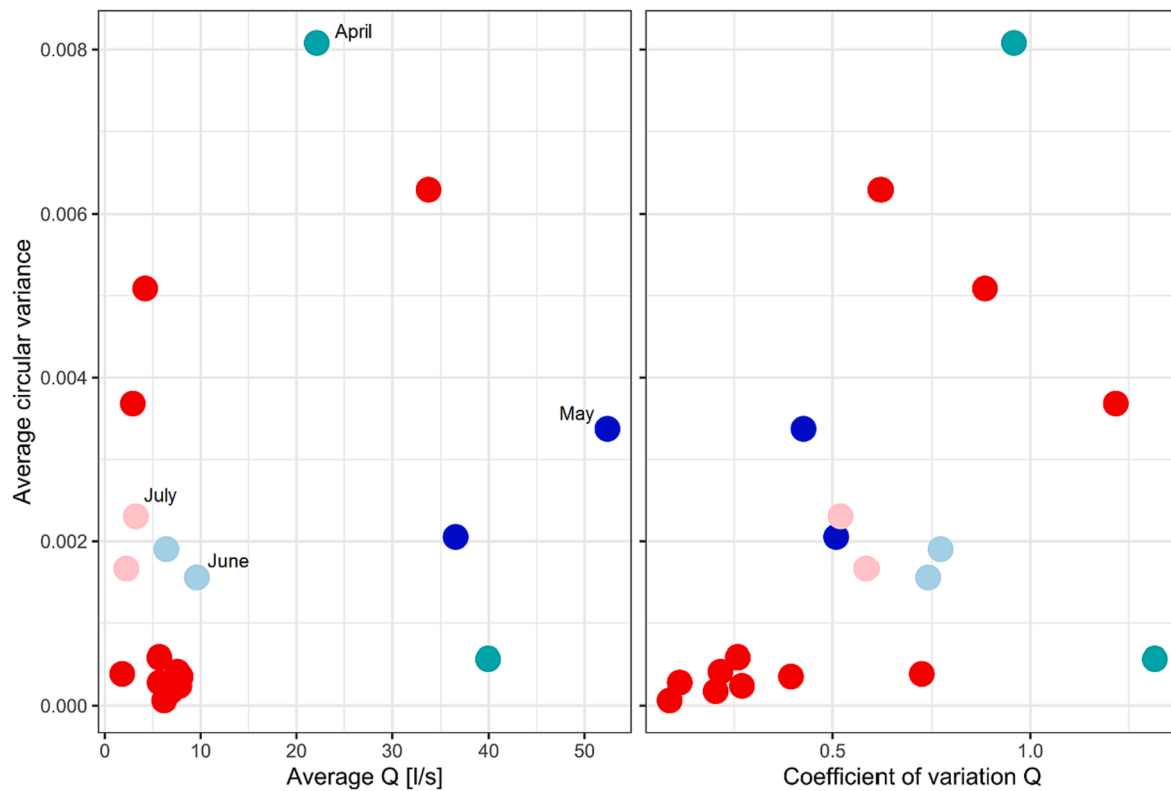The calculated groundwater gradient directions for a small triplet

Fig. 10. Relation between the circular variance of the gradient directions (C_v) for each month and monthly average streamflow (left) or the coefficient of variation of the streamflow for that month (right) for area A. The peak snowmelt period (May) is shown with a dark blue symbol, June with a light blue symbol, April with a green symbol and July with pink symbol. The remaining months are shown with red symbols. (For interpretation of the references to colour in this figure legend, the reader is referred to the web version of this article.)

rarely matched the gradient direction of the surface topography of the original DEM (Fig. 7). For most of the calculated gradients, the directions were less toward the south and more toward the east than the direction calculated from the DEM (Fig. 8). The difference between the mode of the calculated flow directions (i.e., the most frequently occurring flow direction) and the gradient direction of the original DEM (i.e., the difference between the red dot and darkest line in Fig. 7) varied between 14° and 112° (average: 55; median: 41°) for the small triplets. For the large triplets, the difference varied between 0° and 171° (average: 31°; median: 24°). In other words, the discrepancy was smaller for the large triplets.

The variation in the gradient directions (C_v) was larger for the 15 smoothed DEMs than for the observed groundwater gradient directions for both the small triplets (Fig. 11) and the large triplets (Fig. D1 and Fig. D2). The $Gauss_{20}$ and $Mean_5$ DEMs represented the average monthly flow direction for the small triplets best (Table 1). The more smoothed DEMs better represented the gradient directions for the large triplets (Table 2). For the large triplets, the Agg_{10} and Agg_{20} DEMs represented the gradient direction best. The $Gauss_{20}$ and the $Original$ DEM were the third and fourth best DEM in terms of matching the gradient directions for the large triplets, respectively. However, the $Mean_{21}$ and $Gauss_{10}$ DEMs represented the observed gradient directions for the large triplets during the snowmelt in May (in 2019 and 2020) better.

5. Discussion

5.1. How variable are groundwater gradients?

5.1.1. Gradient magnitude

The groundwater gradients of the small and large triplets were correlated to streamflow. Gradient magnitudes were generally higher (i. e., the slope of the water table was steeper) during the snowmelt period

and large or intense rainfall events. However, there were exceptions (e. g., triplet Alt73 in Fig. 9). For these locations, the topographic surface was relatively flat (e.g., 3.8° for Alt73), and the groundwater table was uniformly close to the surface, leading to a low gradient magnitude, even though the overall slope of the groundwater table for the catchment and the surrounding area was steeper.

Visual inspection of the time series of the gradient magnitude showed that it increased faster for the small triplets than the large ones. We assume that this difference in the timing between the small and large triplets is at least in part due to the location of the triplets because more small triplets were located close to the stream where the groundwater was close to the surface. For the small triplets further away from the stream, often, at least one well was dry. Therefore, the data from the small triplets over-represent the dynamics in the more responsive riparian areas. Another potential reason is that the smaller triplets captured faster responses and more small scale variations in the groundwater level that were smoothed out over the larger distances covered by the large triplets.

5.1.2. Gradient direction

As reported in other studies (e.g., Covino and McGlynn, 2007; Heeren et al., 2014; Hinton et al., 1993; Rinderer et al., 2017; Seibert et al., 2003), the groundwater level responded quicker to snowmelt and precipitation events in wells located closer to the stream, where the water level at the beginning of an event was already close to the surface, than in wells further away from the stream, where the groundwater table was deeper. The recessions were also slower for the wells further away from the stream. This difference in response timing can lead to a change in the gradient magnitude and a reversal in the gradient direction. This was observed for a few triplets, e.g., Ast 4 and Alt73 (Fig. 4 and Fig. 5). The maximum change in the gradient direction was 360° for the small triplets and around 270° for the large triplets. This variability is similar
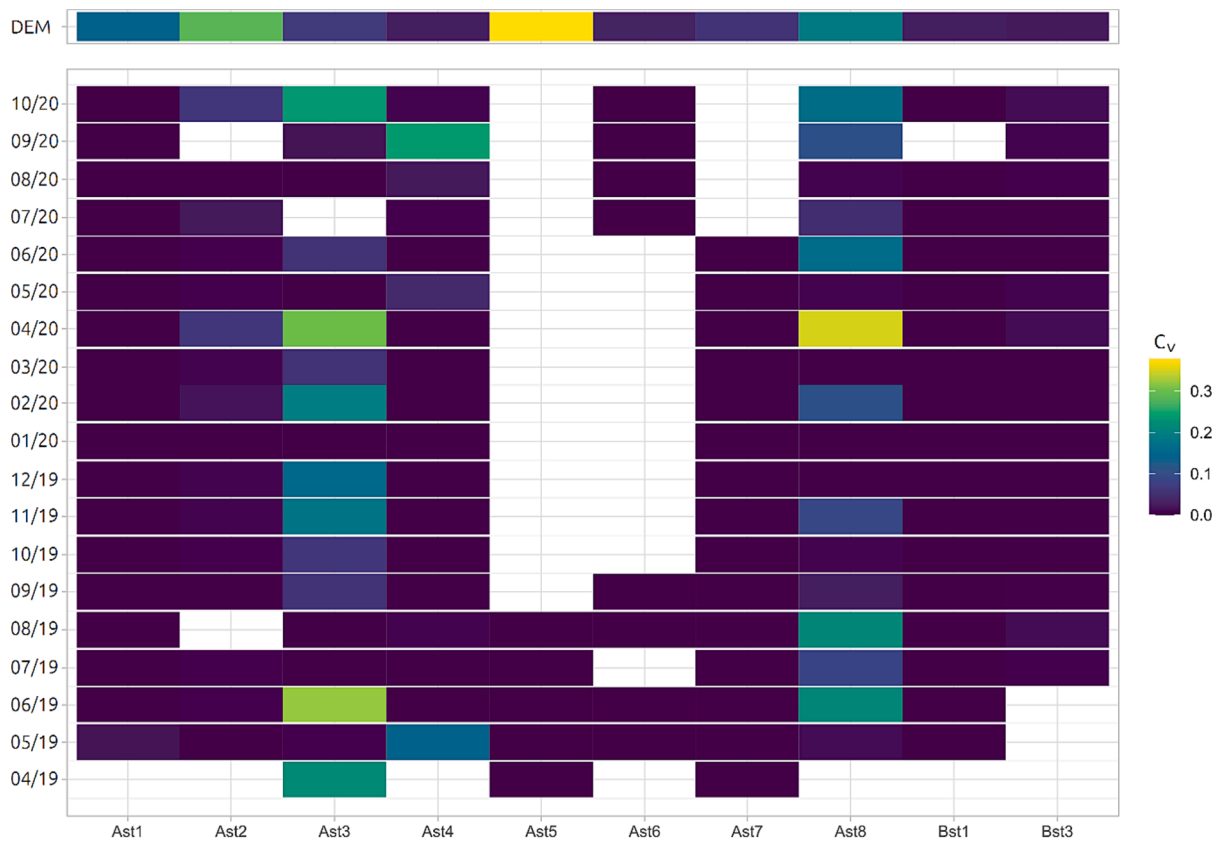
Fig. 11. The circular variance (C_v) of the groundwater gradient direction for each month and for the 15 (smoothed) DEMs (from Erdbrügger et al., 2021; top row) for each small triplet. Missing values for a particular month are indicated in white (i.e., the gradient direction could not be determined for more than three days of the month, either due to data gaps or because the water level dropped below one of the wells). For the results for the large triplets see Figures D1 and D2.

Table 1
Number of small triplets for which the DEM best matched the observed groundwater gradient direction for each month, with the maximum for each month shown in bold font (maximum possible: 9). See Table C1 for a description of the DEMs.

Month	original	gauss$_2$	gauss$_3$	gauss$_5$	gauss$_{10}$	gauss$_{20}$	mean$_3$	mean$_5$	mean$_9$	mean$_{21}$	agg$_2$	agg$_3$	agg$_5$	agg$_{10}$	agg$_{20}$
Apr 19	**1**	0	0	0	0	0	0	**1**	0	**1**	0	0	0	0	0
May 19	**2**	0	0	0	0	**2**	0	0	1	**2**	0	1	0	1	0
Jun 19	1	0	0	0	1	1	1	1	1	1	0	1	1	0	0
Jul 19	1	0	0	**2**	1	**2**	0	1	0	0	0	0	0	1	1
Aug 19	0	0	0	0	0	**2**	1	1	1	1	0	0	0	**2**	1
Sep 19	0	0	1	0	1	**2**	1	1	1	0	0	0	0	**2**	0
Oct 19	1	1	1	0	1	**2**	0	1	0	0	0	0	0	1	0
Nov 19	1	1	0	0	1	**2**	0	**2**	0	0	1	0	0	0	0
Dec 19	0	1	0	0	1	2	0	**3**	0	0	0	0	0	1	0
Jan 20	1	0	0	0	1	2	0	**3**	0	0	0	0	0	1	0
Feb 20	1	0	0	0	1	2	0	**2**	0	0	**2**	0	0	0	0
Mar 20	1	0	0	0	1	2	0	**3**	0	0	0	0	0	1	0
Apr 20	0	0	0	1	1	2	0	**4**	0	0	0	0	0	0	0
May 20	0	0	0	0	0	**2**	0	**2**	0	**2**	0	0	0	1	1
Jun 20	0	1	0	1	1	**2**	0	**2**	0	0	0	1	0	0	0
Jul 20	1	1	0	0	1	**3**	0	1	0	0	0	0	0	0	0
Aug 20	0	0	0	0	1	**3**	0	1	0	0	0	0	0	**2**	1
Sep 20	0	0	0	0	0	**2**	0	1	1	0	0	0	0	1	1
Oct 20	0	0	1	0	1	**4**	0	1	0	1	0	0	0	0	0

to the 284° reported by van Meerveld et al. (2015) but much larger than the values reported in other studies (75° in Rodhe and Seibert (2011) and 61° in Benton et al. (2022). However, for most triplets, the range was much smaller. The median change in gradient direction was around 160° for the small triplets and 45° for the large triplets. The median values of the large triplets are more in line with the values reported in other studies: 25-30° in Rodhe and Seibert (2011), 56° in Benton et al. (2022), and 26° in van Meerveld et al. (2015).

Although we expected the variation in flow directions to be largest

when the streamflow varied most (and wetness conditions were most variable), we did not find this correlation (Fig. 10b). The average variability in the gradient direction (as represented by the average of the C_v) was highest in April 2020 and other wet months. Still, it was not well correlated to the monthly average discharge (Fig. 10a).

5.2. Where are groundwater flow directions most variable?

We expected the groundwater flow directions to be most variable in

Table 2
Number of large triplets for which the DEM best matched the observed groundwater gradient direction for each month, with the maximum for each month shown in bold font (maximum possible: 94 triplets). See Table C1 for a description of the DEMs.

Month	original	gauss$_2$	gauss$_3$	gauss$_5$	gauss$_{10}$	gauss$_{20}$	mean$_3$	mean$_5$	mean$_9$	mean$_{21}$	agg$_2$	agg$_3$	agg$_5$	agg$_{10}$	agg$_{20}$
Apr 19	1	0	1	1	**7**	2	2	1	2	**7**	1	1	1	1	2
May 19	8	1	3	4	11	5	6	2	3	**16**	6	2	2	13	4
Jun 19	5	1	5	2	4	3	4	2	2	**7**	4	3	0	3	3
Jul 19	6	2	1	3	3	3	3	1	2	5	2	2	1	**8**	7
Aug 19	6	1	0	1	2	8	3	1	1	5	3	3	1	7	**10**
Sep 19	6	2	0	1	3	10	3	1	1	5	3	1	3	8	**15**
Oct 19	5	0	1	2	3	4	2	1	1	4	3	0	2	**9**	9
Nov 19	5	1	0	2	3	4	2	2	1	4	4	0	1	**9**	8
Dec 19	3	0	1	1	2	7	1	1	1	1	4	0	1	**11**	4
Jan 20	2	0	1	1	1	5	1	2	1	1	3	0	0	**7**	5
Feb 20	5	0	1	1	1	6	1	2	1	1	3	0	1	**9**	9
Mar 20	4	0	1	1	2	7	1	1	1	1	4	0	1	**10**	7
Apr 20	8	1	1	1	5	8	2	0	2	4	7	0	1	**10**	5
May 20	11	2	1	8	13	7	6	5	6	**15**	4	4	0	6	4
Jun 20	8	3	2	4	7	7	**10**	3	2	9	3	2	3	5	4
Jul 20	6	1	0	1	5	8	3	0	0	5	3	2	1	8	**10**
Aug 20	5	0	0	3	2	4	3	1	1	5	4	2	2	**10**	8
Sep 20	6	0	1	1	1	7	4	1	0	4	3	0	0	6	**8**
Oct 20	**10**	0	4	1	**10**	5	**10**	2	5	8	4	1	4	8	5

flat areas, such as the near stream areas. Indeed, we found a statistically significant negative correlation between the variability in gradient direction (C_v) and the magnitude of the surface gradient (i.e. less variability in the groundwater gradients on steeper slopes). The correlation with the surface gradient magnitude was less clear for the larger triplets because it usually included several smaller-scale topographic features that may cancel each other out. Furthermore, the correlation for the small triplets may be affected by the larger number of triplets in the riparian zone.

There was no significant correlation between C_v and TWI, suggesting that flat areas near the ridges, which typically have a low TWI, and flat areas near the streams, which usually have a high TWI, are both locations of highly variable groundwater directions (cf. Erdbrügger et al., 2021). Unfortunately, the wells near the ridges were frequently dry, which hindered the calculation of the variability in the groundwater flow directions at these sites. Thus, we could not determine if the groundwater flow directions were highly variable at these often somewhat flatter sites throughout the year. The lack of correlation with TWI suggests this may be the case. Still, we have insufficient information to confirm this for particular sites due to the missing data and the bias of the data for these areas to wet conditions.

We observed a general trend of the groundwater gradients being towards the streams during wet periods (such as the snowmelt period and after large precipitation events) and more parallel to the streams (i.e., following the overall trend in topography) during drier periods, as also noted in other studies (e.g., Rodhe and Seibert, 2011; von Freyberg et al., 2014). A noticeable exception were the small triplets close to the streams, where gradients tended to turn (perpendicularly) away from the streams during wet periods and were more parallel or towards the streams during dry periods.

A potential reason for the large variability in the groundwater flow directions (high C_v) for triplets Ast3 and Ast8 (compared to the other triplets) could be their location close to the stream. Water infiltrating from the stream into the near stream aquifer has been well documented in other studies (e.g., Bonanno et al., 2021; Covino and McGlynn, 2007; Heeren et al., 2014; Rodhe and Seibert, 2011; Vidon and Smith, 2007; Winter et al., 2008). Water from further upstream could have flown into the riparian aquifer at some locations (e.g., triplets Ast3 and Ast8) and sufficiently changed the gradient to "overwrite" the gradient resulting from the topography. The effect of the stream was most apparent for the small triplets closest to the stream, probably because of the shorter distances between the wells. Another potential factor could be the level of incision of the streambed into the landscape.

5.3. Which DEM best describes the groundwater flow directions?

Comparing the gradient directions calculated from the groundwater measurements with those calculated for the differently smoothed DEMs suggests that the smoother DEMs match the observed gradients for the large triplets better than the original DEM. The aggregated DEMs describe the observed water table directions best, except during the snowmelt periods when the mean smoothed DEM best matched the observations (see Table 2). The shift in the best DEM during the snowmelt period suggests that despite the lack of correlation between the variability in the gradient direction and streamflow, the best choice of the DEM indeed depends on the wetness status of the catchment.

Thus, to approximate groundwater gradients over distances of around 20 m, we recommend using smoothed DEMs (matched to the season) for the Krycklan catchment and similar catchments. Because the variability in the flow directions for the different DEMs was larger than those calculated from the groundwater levels for most large triplets (Figure D1 and Figure D2), we suggest to use the differences in the gradient directions of strongly smoothed DEMs (rather than all the DEMs of Erdbrügger et al. (2021)) to obtain a first approximation of the potential variability in the groundwater gradient directions.

The small number of small triplets made it difficult to determine the best DEM at the 5 m scale. The relatively smoothed DEM (Gaussian filter, 20 pixels) and a less smoothed DEM (Mean smoothing, 5 pixels) appear suitable. To capture of the overall variation in gradient directions, a distinction may have to be made between near stream locations and locations further upslope because of the different responses of near stream wells and those further away (cf. Haught and van Meerveld, 2011; Rodhe and Seibert, 2011; van Meerveld et al., 2015).

6. Conclusions

Representing the groundwater flow directions correctly is important when determining the size of the groundwater watershed or the directions of water and pollutant transport. Therefore, we used groundwater level data from 75 wells to determine the groundwater gradients and flow directions for nine small (5 m) and 94 large (20 m) triplets. The gradient magnitude of the shallow groundwater changed with catchment wetness. The gradient directions also varied with wetness conditions, especially for near-stream locations. The maximum (and median) range in the groundwater gradient direction was 360° (160°) for the small triplets (5 m distance between wells) and 270° (45°) for the large triplets (20 m distance). Although the monthly variations in the gradient directions were not related to the streamflow variations, they were

highest for the snowmelt period and wet months. For smaller distances, the location relative to the stream needs to be considered as the stream level can significantly affect the groundwater gradients in the near stream areas. While this needs to be further studied, we expect that DEMs with some degree of smoothing better represent the shallow groundwater gradient directions than high resolution DEMs for similar catchments in humid climates with till soils.

CRediT authorship contribution statement

Jana Erdbrügger: Conceptualization, Methodology, Software, Formal analysis, Investigation, Data curation, Writing – original draft, Writing – review & editing, Visualization. **Ilja van Meerveld:** Conceptualization, Methodology, Writing – original draft, Writing – review & editing. **Jan Seibert:** Conceptualization, Methodology, Writing – review & editing, Funding acquisition. **Kevin Bishop:** Conceptualization, Methodology, Writing – review & editing, Funding acquisition.

Declaration of Competing Interest

The authors declare the following financial interests/personal relationships which may be considered as potential competing interests: Jana Erdbrügger reports financial support was provided by Svensk Kärnbränslehantering AB. Jana Erdbrügger reports administrative

Data availability

The field data are available from Erdbrügger et al. (2022) and are described in Erdbrügger et al. (2023).

Acknowledgments

Appendix A:. Gradient calculations

We first calculated the normal vector for a plane through three points:

$$\begin{pmatrix} n_x \\ n_y \\ n_z \end{pmatrix} = \begin{pmatrix} z_2^* \\ z_3^* \\ x_3^* \end{pmatrix} * \begin{pmatrix} y_3^* \\ x_2^* \\ y_2^* \end{pmatrix} - \begin{pmatrix} z_3^* \\ z_2^* \\ x_2^* \end{pmatrix} * \begin{pmatrix} y_2^* \\ x_3^* \\ y_3^* \end{pmatrix} \tag{A1}$$

where:

$$\begin{pmatrix} x_2^* \\ y_2^* \\ z_2^* \end{pmatrix} = \begin{pmatrix} x_2 \\ y_2 \\ z_2 \end{pmatrix} - \begin{pmatrix} x_1 \\ y_1 \\ z_1 \end{pmatrix} \ and \ \begin{pmatrix} x_3^* \\ y_3^* \\ z_3^* \end{pmatrix} = \begin{pmatrix} x_3 \\ y_3 \\ z_3 \end{pmatrix} - \begin{pmatrix} x_1 \\ y_1 \\ z_1 \end{pmatrix} \tag{A2}$$

From the normal vector, we calculated the gradient magnitude (θ) and direction (α) of the normal plane (in degree (°)).

The gradient magnitude (θ) is:

$$\theta = 90 - \left| \arctan\left(\frac{n_z}{\sqrt{n_x^2 + n_y^2}} \right) * \frac{180}{\pi} \right|; 0 < n_z < 0 \tag{A3}$$

and the gradient direction (α) is:

$$\alpha = \begin{cases} \arctan\left(\frac{-n_y}{-n_x} \right) * \frac{180}{\pi}; n_z < 0 \\ \arctan\left(\frac{n_y}{n_x} \right) * \frac{180}{\pi}; n_z > 0 \end{cases} \tag{A4}$$

$n_z = 0$; flat area, zero gradient

The gradient values were assigned to the centroid of the three wells used for the respective calculation, which is calculated as follows:

$$centroid(\overline{x}, \overline{y}) = \left(\frac{x_1 + x_2 + x_3}{3}, \frac{y_1 + y_2 + y_3}{3} \right) \tag{A5}$$

where x_1 and y_1 are the coordinates for the three wells.

Appendix B:. Well triplets and number of measurements for which the gradient could be calculated

Table B1
Number of measurements between July 2019 – July 2020 (max: 52,560 measurements). Triplets with less than two weeks of data (<2016 data points) were excluded from the analyses.

	Triplet	Number of measurements
Small	Ast1	49,189
	Ast2	34,966
	Ast3	40,472
	Ast4	46,747
	Ast5	1,072
	Ast6	20
	Ast7	48,991
	Ast8	50,080
	Bst1	42,281
	Bst3	49,774
Large	Alt1	48,869
	Alt10	50,790
	Alt100	2,159
	Alt101	2,158
	Alt102	2,983
	Alt103	2,920
	Alt104	12,392
	Alt105	12,329
	Alt11	40,473
	Alt15	1,729
	Alt16	1,729
	Alt17	19,608
	Alt18	1,729
	Alt19	25,307
	Alt2	48,947
	Alt20	25,304
	Alt21	1
	Alt22	1
	Alt24	1
	Alt27	45,354
	Alt28	50,230
	Alt29	19,678
	Alt3	40,465
	Alt30	25,396
	Alt31	50,228
	Alt32	25,393
	Alt34	46,397
	Alt35	52,123
	Alt36	52,120
	Alt37	25,382
	Alt38	24,127
	Alt39	1,073
	Alt4	40,892
	Alt5	1,730
	Alt6	1,727
	Alt7	1,727
	Alt73	20,649
	Alt74	20,648
	Alt8	1,727
	Alt84	39,273
	Alt85	40,566
	Alt86	40,484
	Alt87	49,798
	Alt88	50,295
	Alt89	52,377
	Alt9	50,712
	Alt90	50,149
	Alt91	10,175
	Alt92	9,674
	Alt93	52,451
	Alt94	9,675
	Alt95	52,460
	Alt96	2,983
	Alt97	2,161
	Alt98	2,160
	Alt99	2,159
	Blt1	7,174
	Blt10	6,756
	Blt11	12,153
	Blt12	12,749
	Blt13	12,189
	Blt14	6,755

Table B1 (*continued*)

Triplet	Number of measurements
Blt15	12,750
Blt16	12,748
Blt17	6,755
Blt18	49,851
Blt19	50,871
Blt2	7,174
Blt20	50,796
Blt21	19,117
Blt22	8,979
Blt23	51,486
Blt24	8,980
Blt25	19,117
Blt26	8,979
Blt27	52,506
Blt28	8,980
Blt29	19,117
Blt3	12,610
Blt30	8,979
Blt31	50,859
Blt32	8,980
Blt33	19,117
Blt34	8,979
Blt35	19,116
Blt36	19,117
Blt37	19,117
Blt38	19,118
Blt39	49,009
Blt4	12,784
Blt40	7,515
Blt5	6,756
Blt6	10,759
Blt7	8,980
Blt8	46,997
Blt9	6,756

Appendix C

Table C1
DEM names, smoothing method and step, and resolution. Color refers to the color used to represent the DEM in Figs. 4 and 5. The original DEM was obtained from Laudon et al. (2021, 2013).

DEM Name	Color	Smoothing Method	Smoothing Step	Resolution
Original	black	–	–	2 m × 2 m
Gauss$_2$	orange	Gaussian filter	Standard deviation 2x2 pixel	2 m × 2 m
Gauss$_3$		Gaussian filter	Standard deviation 3x3 pixel	2 m × 2 m
Gauss$_5$		Gaussian filter	Standard deviation 5x5 pixel	2 m × 2 m
Gauss$_{10}$		Gaussian filter	Standard deviation 10x10 pixel	2 m × 2 m
Gauss$_{20}$		Gaussian filter	Standard deviation 20x20 pixel	2 m × 2 m
Mean$_3$	blue	mean filter	Window size 3x3 pixel	2 m × 2 m
Mean$_5$		mean filter	Window size 5x5 pixel	2 m × 2 m
Mean$_9$		mean filter	Window size 9x9 pixel	2 m × 2 m
Mean$_{21}$		mean filter	Window size 21x21 pixel	2 m × 2 m
Agg$_2$	green	Aggregation	2 × 2 pixel	4 m × 4 m
Agg$_3$		Aggregation	3 × 3 pixel,	6 m × 6 m
Agg$_5$		Aggregation	5 × 5 pixel	10 m × 10 m
Agg$_{10}$		Aggregation	10 × 10 pixel	20 m × 20 m
Agg$_{20}$		aggregation	20 × 20 pixel	40 m × 40 m

Appendix D:. Comparison of estimated circular variance from DEM and measurements for the large triplets
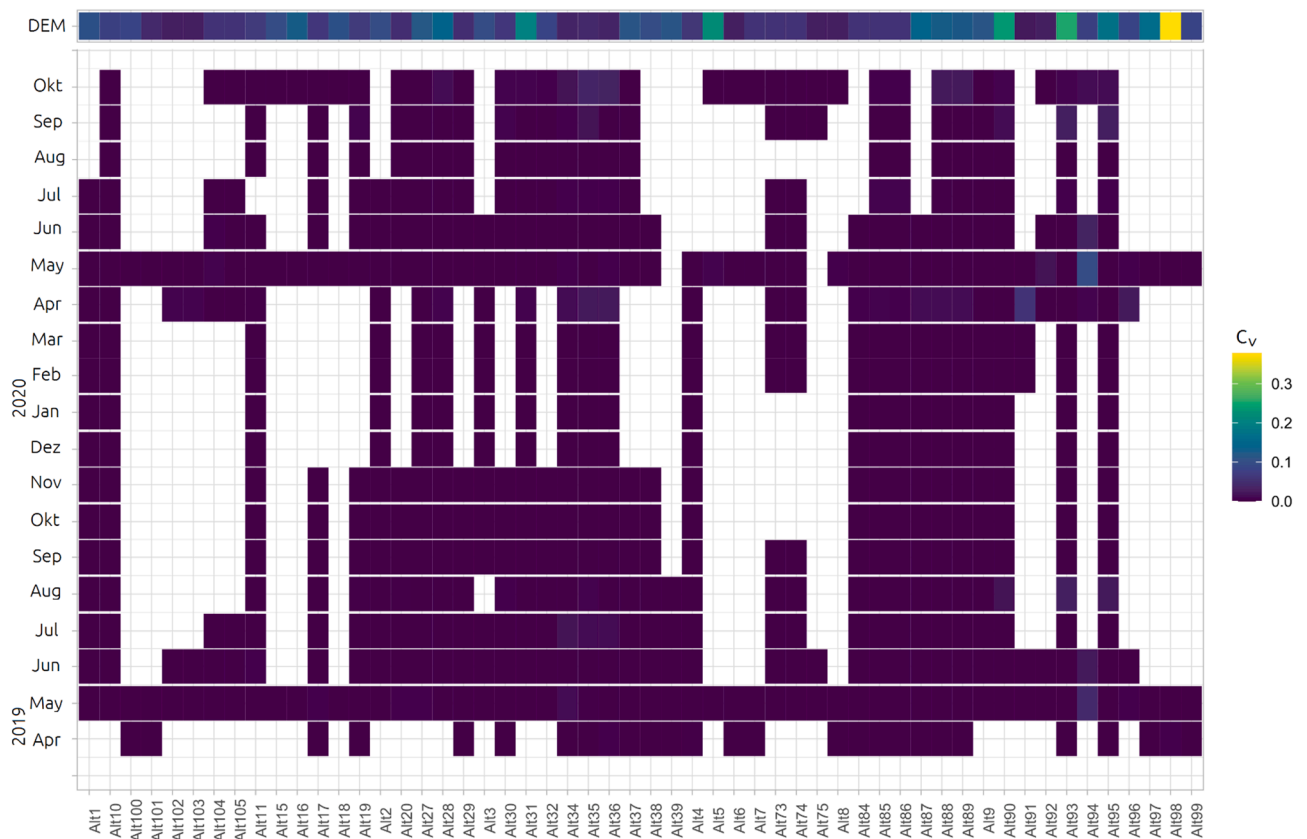

Fig. D1. The circular variance (C_v) of the groundwater gradient direction for each month and for the 15 different smoothed DEMs (top row) for each large triplet in area A. Missing values for a particular month are indicated in white (i.e., the gradient direction could not be determined for more than three days of the month, either due to data gaps or because the water level dropped below one of the wells).
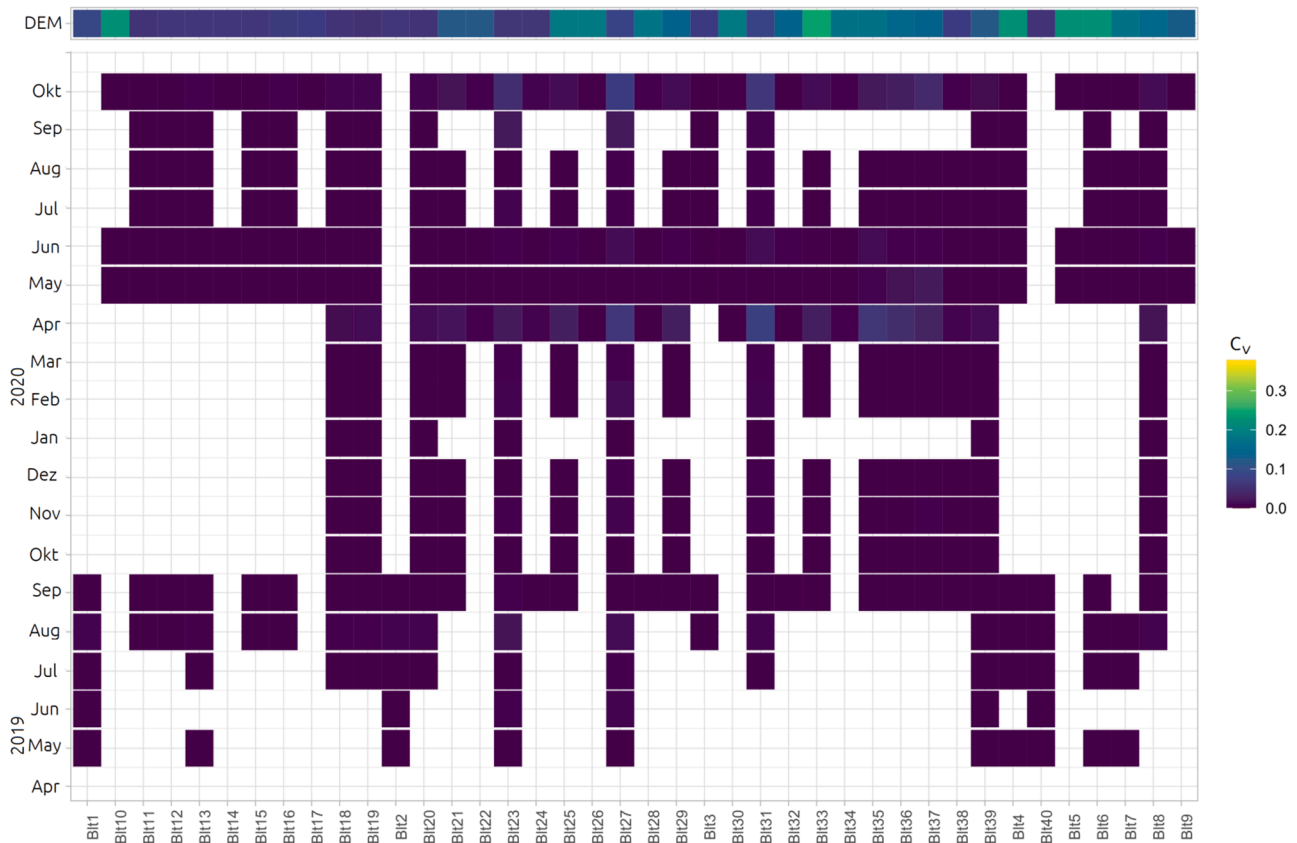
Fig. D2. The circular variance (C_v) of the groundwater gradient direction for each month and for the 15 different smoothed DEMs (top row) for each large triplet in area B. Missing values for a particular month are indicated in white (i.e., the gradient direction could not be determined for more than three days of the month, either due to data gaps or because the water level dropped below one of the wells).

References

Bachmair, S., Weiler, M., Troch, P.A., 2012. Intercomparing hillslope hydrological dynamics: Spatio-temporal variability and vegetation cover effects. Water Resour. Res. 48, 1–18. https://doi.org/10.1029/2011WR011196.

Benton, J.R., McGuire, K.J., Schreiber, M.E., 2022. Subsurface permeability contrasts control shallow groundwater flow dynamics in the critical zone of a glaciated, headwater catchment. Hydrol. Process. 1–16 https://doi.org/10.1002/hyp.14672.

Bonanno, E., Blöschl, G., Klaus, J., 2021. Flow directions of stream-groundwater exchange in a headwater catchment during the hydrologic year. Hydrol. Process. 35, 1–18. https://doi.org/10.1002/hyp.14310.

Condon, L.E., Maxwell, R.M., 2015. Water Resources Research. Water Resour. Res. 51, 6602–6621. https://doi.org/10.1111/j.1752-1688.1969.tb04897.x.

Covino, T.P., McGlynn, B.L., 2007. Stream gains and losses across a mountain-to-valley transition: Impacts on watershed hydrology and stream water chemistry. Water Resour. Res. 43, 1–14. https://doi.org/10.1029/2006WR005544.

Dataflow Systems Ltd, 2021. Odyssey Capacitance Water Level Logger [WWW Document]. URL http://odysseydatarecording.com/index.php?route=product/product&path=59&product_id=50.

Erdbrügger, J., van Meerveld, I., Bishop, K., Seibert, J., 2021. Effect of DEM-smoothing and -aggregation on topographically-based flow directions and catchment boundaries. J. Hydrol. 602, 126717 https://doi.org/10.1016/j.jhydrol.2021.126717.

Erdbrügger, J., van Meerveld, I., Seibert, J., Bishop, K., 2022. Shallow groundwater level time series and groundwater chemistry survey data from Krycklan catchment. GFZ Data Serv. https://doi.org/10.5194/essd-2022-114.

Erdbrügger, J., van Meerveld, I., Seibert, J., Bishop, K., 2023. Shallow-groundwater-level time series and a groundwater chemistry survey from a boreal headwater catchment, Krycklan, Sweden. Earth Syst. Sci. Data 15, 1779–1800. https://doi.org/10.5194/essd-15-1779-2023.

Haitjema, H.M., Mitchell-Bruker, S., 2005. Are water tables a subdued replica of the topography? Ground Water 43, 781–786. https://doi.org/10.1111/j.1745-6584.2005.00090.x.

Haught, D.R.W., van Meerveld, H.J., 2011. Spatial variation in transient water table responses: Differences between an upper and lower hillslope zone. Hydrol. Process. 25, 3866–3877. https://doi.org/10.1002/hyp.8354.

Heeren, D.M., Fox, G.A., Fox, A.K., Storm, D.E., Miller, R.B., Mittelstet, A.R., 2014. Divergence and flow direction as indicators of subsurface heterogeneity and stage-

dependent storage in alluvial floodplains. Hydrol. Process. 28, 1307–1317. https://doi.org/10.1002/hyp.9674.

Hinton, M.J., Schiff, S.L., English, M.C., 1993. Physical properties governing groundwater flow in a glacial till catchment. J. Hydrol. 142, 229–249. https://doi.org/10.1016/0022-1694(93)90012-X.

ICOS, 2021. Svartberget [WWW Document]. URL https://www.icos-sweden.se/Svartberget.

Kolbe, T., Marçais, J., de Dreuzy, J.R., Labasque, T., Bishop, K., 2020. Lagged rejuvenation of groundwater indicates internal flow structures and hydrological connectivity. Hydrol. Process. 34, 2176–2189. https://doi.org/10.1002/hyp.13753.

Lagacherie, P., Moussa, R., Cormary, D., Molenat, J., 1996. Effects of DEM data source and sampling pattern on topographical parameters and on a topography-based hydrological model. IAHS-AISH Publ. 191–199.

Laudon, H., Taberman, I., Ågren, A., Futter, M., Ottosson-Löfvenius, M., Bishop, K., 2013. The Krycklan Catchment Study - A flagship infrastructure for hydrology, biogeochemistry, and climate research in the boreal landscape. Water Resour. Res. 49, 7154–7158. https://doi.org/10.1002/wrcr.20520.

Laudon, H., Hasselquist, E.M., Peichl, M., Lindgren, K., Sponseller, R., Lidman, F., Kuglerová, L., Hasselquist, N.J., Bishop, K., Nilsson, M.B., Ågren, A.M., 2021. Northern landscapes in transition: Evidence, approach and ways forward using the Krycklan Catchment Study. Hydrol. Process. 35, 1–15. https://doi.org/10.1002/hyp.14170.

Moges, D.M., Virro, H., Kmoch, A., Cibin, R., Rohith, A.N., Martínez-Salvador, A., Conesa-García, C., Uuemaa, E., 2023. How does the choice of DEMs affect catchment hydrological modeling? Sci. Total Environ. 892 https://doi.org/10.1016/j.scitotenv.2023.164627.

Molénat, J., Gascuel-Odoux, C., Davy, P., Durand, P., 2005. How to model shallow water-table depth variations: The case of the Kervidy-Naizin catchment. France. Hydrol. Process. 19, 901–920. https://doi.org/10.1002/hyp.5546.

Moore, R.D., Thompson, J.C., 1996. Are water table variations in a shallow forest soil consistent with the TOPMODEL concept? Water Resour. Philos. Phenomenol. Res. 32, 663–669. https://doi.org/10.1029/95WR03487.

Myrabø, S., 1997. Temporal and spatial scale of response area and groundwater variation in till. Hydrol. Process. 11, 1861–1880. https://doi.org/10.1002/(sici)1099-1085(199711)11:14<1861::aid-hyp535>3.0.co;2-p.

Pewsey, A., Neuhäuser, M., Ruxton, G.D., 2013. Circular Statistics in R, 1st ed. Oxford University Press, Oxford.

Rinderer, M., van Meerveld, I., Seibert, J., 2014. Topographic controls ond shallow groundwater levels in a steep, prealpine catchment. Water Resour. Res. 50, 6067–6080. https://doi.org/10.1002/2013WR015009.

Rinderer, M., McGlynn, B.L., van Meerveld, H.J., 2017. Groundwater similarity across a watershed derived from time-warped and flow-corrected time series. Water Resour. Res. 53, 3921–3940. https://doi.org/10.1002/2016WR019856.

Rodhe, A., Seibert, J., 2011. Groundwater dynamics in a till hillslope: Flow directions, gradients and delay. Hydrol. Process. 25, 1899–1909. https://doi.org/10.1002/hyp.7946.

Seibert, J., Bishop, K., Rodhe, A., McDonnell, J.J., 2003. Groundwater dynamics along a hillslope: A test of the steady state hypothesis. Water Resour. Res. 39, 1–9. https://doi.org/10.1029/2002WR001404.

Tóth, J., 1962. A Theory of Groundwater Motion in Small Drainage Basins. J. Geophys. Res. 67.

Tromp-van Meerveld, H.J., McDonnell, J.J., 2006. Threshold relations in subsurface stormflow: 1. A 147-storm analysis of the Panola hillslope. Water Resour. Res. 42, 1–11. https://doi.org/10.1029/2004WR003778.

van Meerveld, H.J., Seibert, J., Peters, N.E., 2015. Hillslope-riparian-stream connectivity and flow directions at the Panola Mountain Research Watershed. Hydrol. Process. 29, 3556–3574. https://doi.org/10.1002/hyp.10508.

Vidon, P., 2012. Towards a better understanding of riparian zone water table response to precipitation: Surface water infiltration, hillslope contribution or pressure wave processes? Hydrol. Process. 26, 3207–3215. https://doi.org/10.1002/hyp.8258.

Vidon, P., Smith, A.P., 2007. Upland controls on the hydrological functioning of riparian zones in glacial till valleys of the midwest. J. Am. Water Resour. Assoc. 43, 1524–1539. https://doi.org/10.1111/j.1752-1688.2007.00125.x.

von Freyberg, J., Radny, D., Gall, H.E., Schirmer, M., 2014. Implications of hydrologic connectivity between hillslopes and riparian zones on streamflow composition. J. Contam. Hydrol. 169, 62–74. https://doi.org/10.1016/j.jconhyd.2014.07.005.

Winter, T.C., 1999. Relation of streams, lakes, and wetlands to groundwater flow systems. Hydrgeol. J. 7, 28–45. https://doi.org/10.1007/s100400050178.

Winter, T.C., Buso, D.C., Shattuck, P.C., Harte, P.T., Vroblesky, D.A., Goode, D.J., 2008. The effect of terrace geology on ground-water movement and on the interaction of ground water and surface water on a mountainside near Mirror Lake, New Hampshire. USA. Hydrol. Process. 22, 21–32. https://doi.org/10.1002/hyp.6593.

Wise, S.M., 2007. Effect of differing DEM creation methods on the results from a hydrological model. Comput. Geosci. 33, 1351–1365. https://doi.org/10.1016/j.cageo.2007.05.003.

Wroblicky, G.J., Campana, M.E., Valett, H.M., Dahm, N., 1998. Seasonal variation in surface-subsurface water exchange and lateral hyporheic area of two stream-aquifer system. Water Resour. 34, 317–328.